Comparative Analysis of UV-assisted Removal of Azithromycin and Cefixime from Aqueous Solution Using PAC/Fe/Si/Zn Nanocomposite

Azadeh Mehrdoost[1], PhD;
Reza Jalilzadeh Yengejeh[1],
PhD; Mohammad Kazem
Mohammadi[2], PhD; Ali Akbar
Babaei[1,3], PhD; Azadeh
Haghighatzadeh[4], PhD

Abstract

Background: Pharmaceutical pollutants are one of the most important pollutants for water resources, and their health and environmental effects have been well estimated. Absorption is one of the best methods of the removal of antibiotics using nanocomposite.

Methods: This experimental study was performed on Nano composites. The PAC/Fe/Si/Zn Nano composite was successfully synthesized using a co-precipitation method in which iron (Fe), silicon (Si) and zinc (Zn) were loaded on the activated carbon powder (PAC). The structural features of the as-synthesized Nano composite were determined using X-ray diffraction (XRD), field emission scanning electron microscopy (FESEM) and energy dispersive X-ray spectroscopy (EDS). The as-synthesized Nano composite was utilized to remove azithromycin and cefixime from aqueous solution with the assistance of UV light. The effect of operational parameters such as pH, irradiation time, initial azithromycin/cefixime concentration and Nano composite dose on UV-assisted removal performance was evaluated using an optimization process.

Results: The UV-assisted removal activities indicated more removal percentage (99.7%) for azithromycin compared to cefixime (95.6%). The kinetics of removal was tested using Langmuir-Hinshelwood model, indicating the first-order reaction kinetics as the best model for UV-assisted removal of both azithromycin and cefixime. Adsorption equilibrium data were modeled using Langmuir and Freundlich isotherms. Azithromycin equilibrium adsorption showed a good fit with both Langmuir and Freundlich models, while the most suitable model for cefixime adsorption was estimated to be Langmuir isotherm.

Conclusion: The findings showed that PAC/Fe/Si/Zn Nano composite were well able to degrade non-biodegradable antibiotics in aqueous solutions, which is very valuable from environmental aspects.

[1]Department of Environmental Engineering, Ahvaz Branch, Islamic Azad University, Ahvaz, Iran;
[2]Department of Chemistry, Ahvaz Branch, Islamic Azad University, Ahvaz, Iran;
[3]Department of Environmental Health Engineering, School of Public Health, Ahvaz Jundishapur University of Medical Sciences, Ahvaz, Iran;
[4]Department of Physics, Ahvaz Branch, Islamic Azad University, Ahvaz, Iran

Correspondence:
Reza Jalilzadeh Yengejeh, PhD;
Department of Environmental Engineering, Ahvaz Branch, Islamic Azad University, Post code: 61349-37333, Post office: 1915, Ahvaz, Iran
Tel: +98 9124794322
Email: r.jalilzadeh@iauahvaz.ac.ir
Received: 5 October 2020
Revised: 1 November 2020
Accepted: 3 December 2020

Introduction

The safety of drinking water and wastewater-treated water has attracted much attention due to the lack of water resources. However, human society is suffering from the adverse outcomes related to the contamination of aquatic systems deriving from domestic, agricultural and industrial activities.[1, 2] The earth's life has been

threatened by pharmaceutical compounds being detected in samples from aqueous environment, such as river water, ground water and drinking water related to the effluent of wastewater treatment plants.[3, 4] Antibiotics, as a main category of widely-used drugs to treat an extensive number of bacterial infections, can be detected in various water bodies as a result of their incomplete absorption during their metabolization and continuous use. It has been revealed that antibiotics can induce the selection of resistant bacterial strains in contact with living beings that would cause diseases untreatable with antibiotics and decreasing the ability to stop epidemics.[5, 6]

Many attempts have been made by different research groups to remove azithromycin ($C_{38}H_{72}N_2O_{12}$) and cefixime ($C_{16}H_{15}N_5O_7S_2$), as broad-spectrum antibiotics, from aquatic environments. In this respect, Muñoz-Calderón et al. presented a report on the use of low frequency ultrasound to treat water from azithromycin.[7] Naraginit et al. described visible light degradation of macrolide antibiotic azithromycin by novel $ZrO_2/Ag@TiO_2$ nanorod composite.[8] Sayadi et al. demonstrated photocatalytic degradation of azithromycin using $GO@Fe_3O_4/ZnO/SnO_2$ nanocomposites.[9] Cano et al. utilized simulated sunlight radiation and hydrogen peroxide in azithromycin removal from water assessing the effects of operational parameters like the initial pH and peroxide concentration.[5] Moreover, Shokri et al. reported removal efficiency of Azithromycin from wastewater using advanced oxidation process and moving- bed biofilm reactor.[10] Salimi et al. reported photocatalytic degradation of cefixime with MIL-125(Ti)-mixed linker decorated by g-C_3N_4 under solar driven light irradiation.[11] Another study by Salimi et al. also described the application of MIL-53(Fe)/urchin-like g-C_3N_4 nanocomposite for efficient degradation of cefixime.[12] Pham et al. explained adsorption characteristics of beta-lactam cefixime onto nanosilica fabricated from rice HUSK with surface modification by polyelectrolyte.[13]

It is believed that UV-assisted degradation lacks applicability for the pharmaceuticals removal in the wastewater treatment systems.[14] However, recently, a considerable amount of literature has been found on the removal of organic pollutants like hydrocarbons and pharmaceuticals with UV treatment. A study on the advanced oxidation of the pharmaceutical drug diclofenac with UV/H_2O_2 and ozone was performed by Vogan et al.[15] Shokri et al. applied UV activation of hydrogen peroxide method for removal of Azithromycin antibiotic from aqueous solution.[16] Kim et al. explained the performance of UV and UV/H_2O_2 processes for the removal of pharmaceuticals detected in the secondary effluent of a sewage treatment plant in Japan.[14] Fu et al. presented a report on mechanisms and efficiency of degradation of three nonsteroidal anti-inflammatory

drugs by UV/Persulfate.[17] Experimental and model comparisons of H_2O_2 assisted UV photodegradation of microcyctin-LR in simulated drinking water were made by Li et al.[18] Application of the UV/sulfoxylate/phenol process in the simultaneous removal of nitrate and pentachlorophenol from the aqueous solution was described by Asgari et al.[19] Janssens et al. performed an investigation on the coupling of nano-filtration and UV, UV/TiO_2 and UV/H_2O_2 processes for the removal of anti-cancer drugs from real secondary wastewater effluent.[20]

In recent years, powder activated carbon (PAC) adsorption has been reported to be an effective material for the removal of pharmaceuticals from wastewater and water streams.[21] However, reports have indicated that the separation of such a material from aqueous solutions has been a main disadvantage, which can be promoted through inducing the magnetic properties.[22] This study focused on the synthesis of PAC/Fe/Si/Zn nanocomposite for the removal of azithromycin and cefixime from aqueous solution with the assistance of UV light. Batch removal experiments were conducted to investigate the effects of the operational factors including pH, irradiation time, initial azithromycin/cefixime concentration, and nanocomposite dose. The UV-assisted removal kinetics was modeled using Langmuir-Hinshelwood functions, while the adsorption equilibrium data were analyzed using Langmuir and Freundlich models. The recycling tests were finally carried out to survey the stability features of the synthesized nanocomposite. To the best of our knowledge, this was the first report on examining the UV-assisted removal properties of PAC/Fe/Si/Zn nanocomposite to decrease azithromycin and cefixime.

Methods

Experimental

All reagents and materials were purchased from Merck. All chemicals were at an analytical grade and utilized without further purifications. Distilled water had been used throughout the experiments.

The X-ray diffraction pattern was obtained using an Ultimate IV Multipurpose X-ray diffractometry system with Cu Kα radiation ($\lambda = 0.15406 nm$) to estimate the crystalline phase. The morphology and composition of the nanoparticles were investigated using a field emission scanning electron microscopy (FESEM, Zeiss SIGMA VP-500) equipped with a high-resolution elemental mapping detector (EDS, SAMAX) and an energy dispersive X-ray spectroscopy (EDX, Oxford Instruments).

Preparation of the Sample

The PAC/Fe/Si/Zn nanocomposite was synthesized

via a three-step process as shown in Figure 1. The first step was to load the iron on the powder activated carbon (PAC) through co-precipitation and reduction techniques.[22] In this stage, FeSO₄.7H₂O (5 g) was first dissolved in a methanolic solution (100 mL) with 30:70 volumetric ratio of methanol to distilled water under constant stirring for 30 min. PAC (5 g) was then added to the obtained mixture and pH was adjusted at 7 with the addition of NaOH (3.8 M). An aqueous NaBH₄ solution obtained through adding NaBH₄ (4 g) to distilled water (100 mL) was added into the above mixture and magnetically stirred for 1 h. The obtained PAC/Fe particles were separated from the liquid phase by a magnet (1.2 T) and washed with acetone for three times. The wet precipitate was finally maintained under N₂-purged environment for 3 h and dried at 30°C for 4 h.

The second step was involved in loading silicon on PAC/Fe particles by a co-precipitation method. In this experiment, as-synthesized PAC/Fe powders (1 g) along with trisodium citrate dehydrate (1 g) were first dissolved in an ethanolic solution (100 mL) with 2.5:1 volumetric ratio of ethanol to distilled water under continuous stirring for 30 min. An ammonia solution (1 mL) and TEOS (1 mL) was then dropped into the above suspension and stirred at 40°C for 3 h. The obtained precipitate was finally collected by a magnet (1.2 T), washed by ethanol, and dried at 60°C for 1 h. The third step was adding Zn to the prepared PAC/Fe/Si (1.5 g) was first dispersed into 99% ethanol (50 mL) and followed by the addition of 0.1 M Zn(NO₃)₂.6H₂O (50 mL) under continuous stirring for 30 min. The final product was collected by a magnet (1.2 T), washed with ethanol, and dried at 120°C for 24 h.

Experimental Removal Procedure

The UV-assisted removal experiments were conducted to reduce azithromycin (AZT) and cefixime (CEF) as model pollutants from aqueous solutions using the PAC/Fe/Si/Zn nanocomposite. In brief, a certain amount of AZT or CEF (100 mg) was first dissolved in methanol (40 mL) under continuous stirring for 30 min followed by the addition of distilled water to reach a 100 mL volume. A typical removal experiment was then carried out in 250 mL of AZT or CEF solution with certain initial concentration, pH, and nanocomposite dosage. The reaction temperature was maintained constant using two fans being set at two sides of the used reactor system. Suspensions were vigorously shaken on a magnetic stirrer under dark conditions for 30 min to reach an adsorption-desorption equilibrium. After that, a UV lamp (UV-C lamp, 254 nm and 6W PHILIPS) was set into the open central region of the sample. A certain amount of solutions (3 mL) was withdrawn every 30 min and centrifuged (3000 *rpm* for 10 *min*) to remove the nanocomposite particles. The concentrations of AZT and CEF were determined by ultraviolet-visible spectroscopy using a UV-Vis spectrophotometer (Hach DR 5000) at a wavelength of 274 and 288 nm, respectively. The equilibrium capacity of nanocomposite in dark was calculated using the following equation:[23]

$$q_e = \frac{(C_0 - C_e)V}{m} \tag{1}$$

where, parameters C_0 and C_e are the initial and equilibrium concentrations of AZT or CEF in mgL⁻¹, respectively. V is the initial solution volume in L and m is the catalyst amount (*g*), respectively. The UV-assisted removal percentages of AZT and CEF were estimated as:[24]
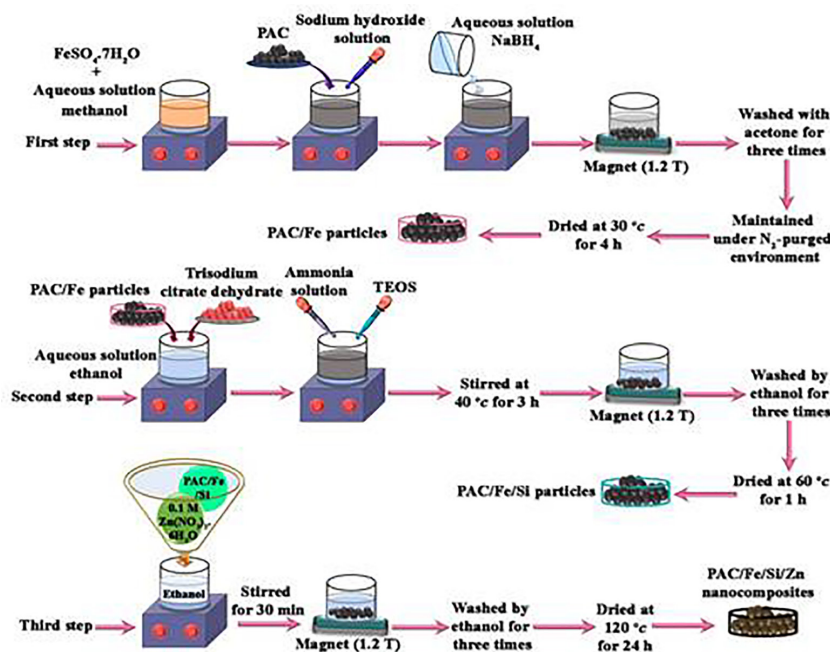
Figure 1: Schematic illustration of synthesis route of the PAC/Fe/Si/Zn nanocomposite

$$D(\%) = \frac{(C_0 - C_t)}{C_0} \times 100 \qquad (2)$$

where, C_0 and C_t are AZT or CEF concentrations after absorption equilibrium in mgL^{-1} at each irradiated time of t, respectively.

Results

Structural Studies

The phase nature of the as-synthesized nanocomposite was investigated using X-ray diffractometery (XRD). Figure 2 shows XRD spectrum of PAC/Fe/Si/Zn sample in 2θ ranging from 20° to 80°. The XRD spectrum of PAC/Fe/Si/Zn sample indicated the presence of PAC crystals by showing the characteristic peaks of 24.12° and 42.47° assigned to 002 and 100 planes of carbon, respectively.[25] The XRD spectrum of the PAC/Fe/Si/Zn nanocomposite also presented reflection peaks at 2θ of 29.46° and 43.47° indexed to 102 and 110 planes of hexagonal SiO$_2$ with space group P63/mmc (00-018-1169). The XRD spectrum of PAC/Fe/Si/Zn sample indicated the presence of hexagonal ZnO structures with space group P63 by showing 100, 002 and 103 planes at 31.83°, 34.45° and 62.71°, respectively (00-036-1451). The results shown in Figure 3 confirmed the presence of C, Si and Zn elements in PAC/Fe/Si/Zn sample. The existence of Fe would be further justified by FESEM-EDS and EDX analysis (Figures 4 and 5).

Field emission scanning electron microscopy (FESEM) analysis was carried out to investigate the morphology of the as-synthesized nanocomposite. Figure 3 illustrates FESEM micrographs of PAC/Fe/Si/Zn sample in two different magnifications. It can be seen in Figure 3a and b that PAC/Fe/Si/Zn
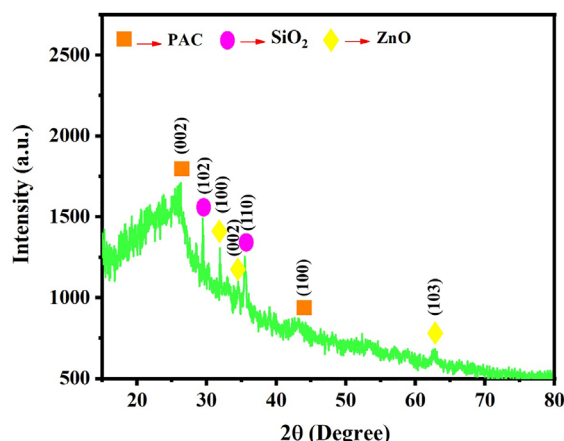
Figure 2: XRD pattern of the PAC/Fe/Si/Zn nanocomposite

sample consisted of a mixed morphology including fiber-like, sphere-like, and irregular shapes. A closer look at high-resolution images shown in Figure 3c and d revealed an average diameter of about 60 nm for fiber-like particles. It is also obvious from Figure 3c and d that the diameter of the c of nanometers is a few micrometers.

The chemical compositional analysis of PAC/Fe/Si/Zn nanocomposite was performed using FESEM-EDS mapping, as shown in Figure 4. It can be seen in Figure 4b that the elemental mapping images illustrated the presence of C, Fe, Si and Zn elements in the boxed surface area (Figure 4a). The result obtained from Figure 4 indicated that Fe, Si and Zn elements were uniformly dispersed on the surface of PAC structures. Figure 5 shows the EDX spectrum of PAC/Fe/Si/Zn sample to estimate the quantitative elemental values. The EDX spectrum shown in Figure 5 revealed the existence of C, Fe, Si and Zn elements with weight percentages presenting in Table 1.
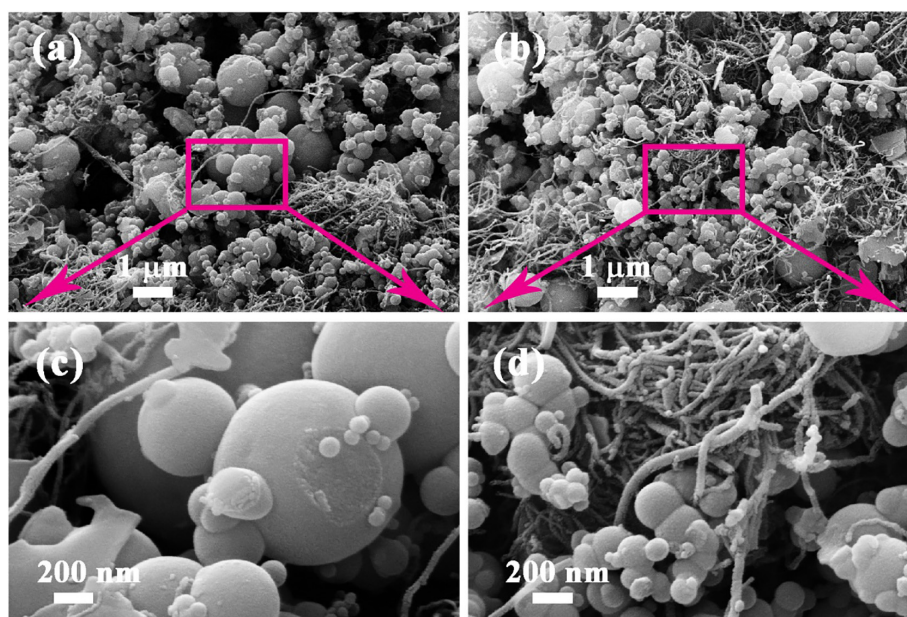
Figure 3: (a,b) low-resolution and (c,d) high-resolution FESEM images of the PAC/Fe/Si/Zn nanocomposite
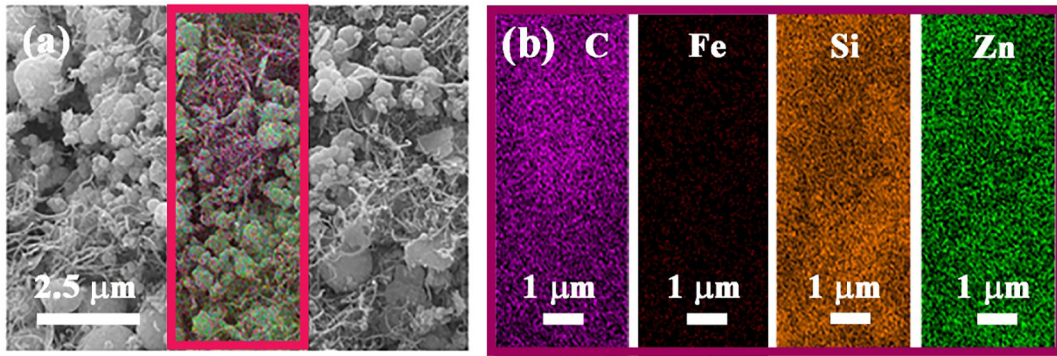
Figure 4: (a) FESEM map image and (b) the corresponding elemental mappings for the PAC/Fe/Si/Zn nanocomposite.
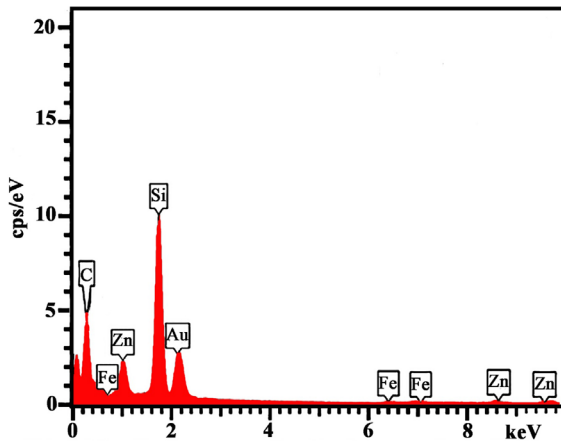
Figure 5: EDX spectrum of the PAC/Fe/Si/Zn nanocomposite

UV-assisted Removal Studies

A series of experiments were carried out to examine the factors affecting UV-assisted removal processes in the batch system. The AZT and CEF removal experiments were performed in the presence of the PAC/Fe/Si/Zn nanocomposite and the results are presented in Figure 6. One of the most important parameters affecting the efficiency of AZT and CEF removal is pH. Figure 6a shows the pH changes (3, 7, 9 and 11) on the removal percentage of AZT and CEF in the presence of PAC/Fe/Si/Zn sample. The experiments were performed for solutions with the initial AZT/CEF concentration of 10 ppm, nanocomposite amount of 0.02g, and irradiation time of 120 min. It can be seen in Figure 6a that the AZT removal percentage increased from 30.0% to 73.2% with increasing pH value from 4 to 9. However, the AZT removal percentage showed a decrease of 48.0% with further increasing pH value of 11. It is obvious from Figure 6a that the CEF removal percentage showed an increasing trend from 32.3% to 72.8% with increasing pH from 4 to 11. Therefore, values equivalent to 9 and 11 were considered as the optimal pH for AZT and CEF removal in the presence of PAC/

Fe/Si/Zn sample.

The effect of UV irradiation time on the AZT and CEF removal in the presence of PAC/Fe/Si/Zn nanocomposite was investigated in regular time intervals of 20 min up to 120 min. The studies were done in solutions with optimal pH and initial AZT/CEF concentration of 10 *ppm* containing 0.02*g* of nanocomposite; the results are shown in Figure 6b. As plotted in Figure 6b, both AZT and CEF removal percentages initially indicated an increase in the presence of PAC/Fe/Si/Zn sample as time prolonged to 120 min. Both AZT and CEF removal percentages then decreased and reached an equilibrium state at irradiation time of 120 min. Figure 6b proposed an optimal time of 120 min in the presence of PAC/Fe/Si/Zn with the removal percentages equal to 61.1% and 81.0% for AZT and CEF, respectively.

The effect of initial concentrations of AZT and CEF on the removal processes was examined by considering the established optimized conditions. The results for samples with initial AZT/CEF concentrations of 10, 20, 30 and 40 ppm after 120 min of UV irradiation are plotted in Figure 6c. It can be seen in Figure 6c that the increase of initial CEF concentration from 10 to 20 ppm increased the removal rate from about 72.8% to 86.4%. However, the further increase of initial CEF concentration to 40 ppm showed a decrease in the removal rate to about 58.3%. It can also be concluded from Figure 6c that the removal rate decreased from 83.2% to 55.6% with increasing initial AZT concentration from 10 to 40 ppm. The obtained results suggested values equal to 20 and 10 ppm for initial CEF and AZT concentrations in the presence of the PAC/Fe/Si/Zn nanocomposite.

The effect of nanocomposite dose on AZT/CEF removal rate was investigated in samples with the established optimal conditions under a UV irradiation period of 120 min. Figure 6d shows the removal AZT and CEF percentages for different nanocomposite

Table 1: Quantitative EDX analysis of the PAC/Fe/Si/Zn nanocomposite

Element	Carbon (C)	Iron (Fe)	Silicon (Si)	Zinc (Zn)
Wt%	52.1	1.6	12.2	34.1
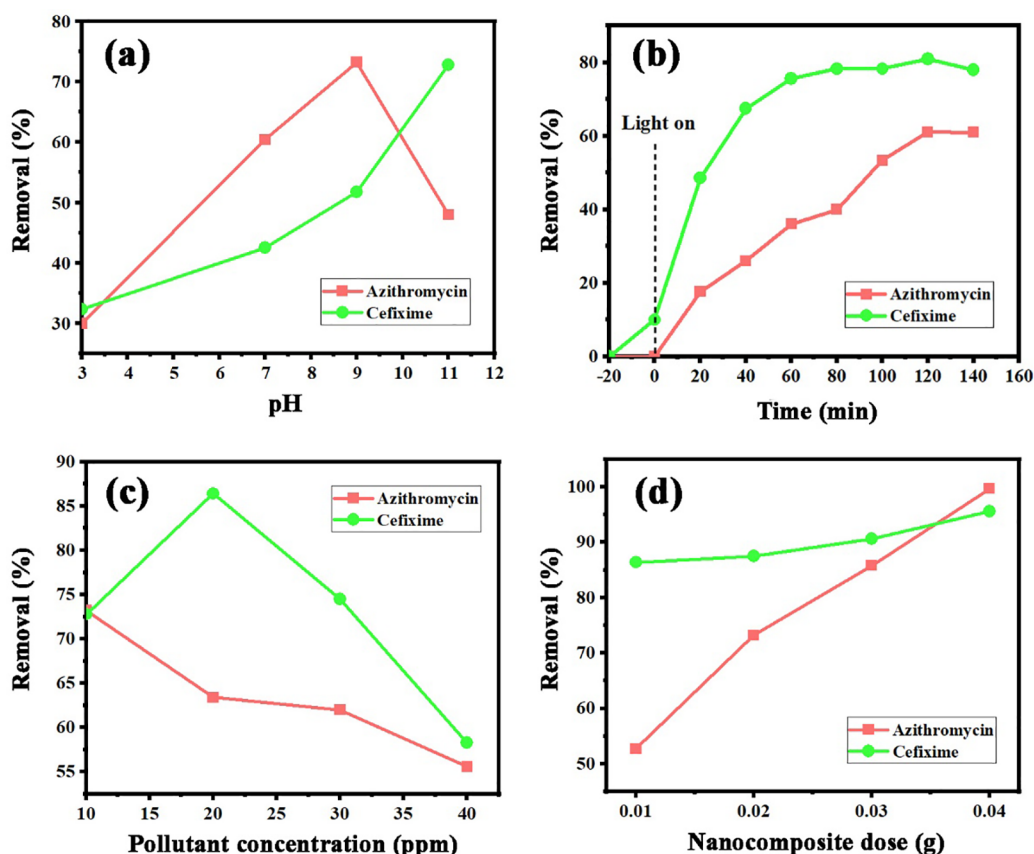
Figure 6: The effect of (a) pH, (b) UV irradiation time, (c) initial AZT/CEF concentration and (d) nanocomposite dose on the AZT/CEF removal in the presence of the PAC/Fe/Si/Zn nanocomposite

amounts (0.01, 0.02, 0.03 and 0.04 g). It is obvious from Figure 6d that an increase in the nanocomposite amount from 0.01 to 0.04 g showed an enhancement from about 52.7% (86.4%) to 99.7% (95.6%) for the removal rate of AZT (CEF). Such a result proposed an optimal amount equivalent to 0.04 g for the PAC/Fe/Si/Zn nanocomposite for AZT/CEF removal.

Langmuir-Hinshelwood model was utilized to investigate the reaction kinetics of UV-assisted removal processes. Langmuir-Hinshelwood model was described based on the following formulas:[26]

$$(C_0 - C_t) = k_0 t \tag{3}$$

$$-\mathrm{h}\left(\frac{C_t}{C_0}\right) = k_1 t \tag{4}$$

$$\left(\frac{1}{C_t} - \frac{1}{C_0}\right) = k_2 t \tag{5}$$

where, parameters of k_0, k_1 and k_2 are the reaction rate constants of zero-, first- and second-order models in $mgL^{-1}min^{-1}$, min^{-1} and $Lmg^{-1}min^{-1}$, respectively. The studies were conducted under optimized conditions determined in UV-assisted AZT/CEF removal processes. Figure 7a-c displays the variations of

$(C_0 - C_t)$, $-\mathrm{h}(C_t / C_0)$ and $(1/C_t - 1/C_0)$

as a function of reaction time, respectively. The reaction kinetic constants (k) were estimated by the slop of theoretically fitted lines to Eqs. (3)-(5) and the best-fitting kinetic model was estimated using the highest correlation coefficients (R^2). The constants of UV-assisted AZT/CEF removal rate and their corresponding correlation coefficients for the PAC/Fe/Si/Zn nanocomposite are listed in Table 2. It can be concluded from Table 3 that the UV-assisted removal reaction of both AZT and CEF followed the first-order reaction kinetics.

It is believed that the stability of a practical nanocomposite is significant in the removal of aqueous pollutants as well as its performance. The recycling experiment was conducted to examine the stability of the PAC/Fe/Si/Zn nanocomposite on the UV-assisted AZT/CEF removal. Figure 8 shows the results of four successive runs for the AZT/CEF removal under estimated optimized conditions. It can be seen in Figure 8 that the UV-assisted removal activities of the recycled PAC/Fe/Si/Zn samples could be well maintained after three times reuse, indicating that the as-synthesized samples had a good stability.
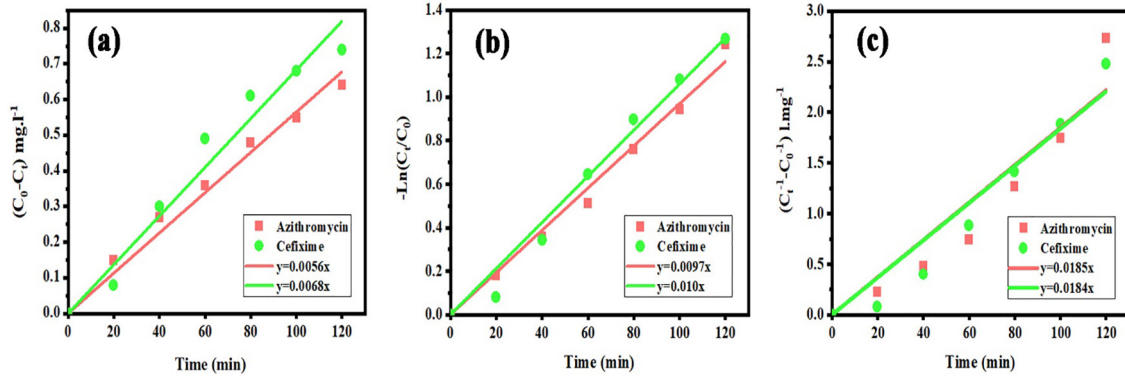
Figure 7: (a) zero-, (b) first- and (c) second-order kinetic curves for UV-assisted AZT/CEF removal in the presence of the PAC/Fe/Si/Zn nanocomposite

Table 2: Kinetic analysis for AZT/CEF using the PAC/Fe/Si/Zn nanocomposite

Pollutant	Zero-order		First-order		Second-order	
	K_0 (mgL^{-1}min^{-1})	R_0^2	K_1 (min^{-1})	R_1^2	K_2 (Lmg^{-1}min^{-1})	R_2^2
AZT	0.0056	0.9946	0.0097	0.9962	0.0185	0.9577
CEF	0.0068	0.9879	0.0100	0.9935	0.0184	0.9743

Table 3: Langmuir and Freundlich isotherm parameters for AZT/CEF adsorption using the PAC/Fe/Si/Zn nanocomposite

Pollutant	Langmuir				Freundlich			
	q_{max} (mgg^{-1})	K_L (Lmg^{-1})	R_L	R^2	$1/n_F$ (gmg^{-1})	n_F (mgg^{-1})	K_F (mgg^{-1})	R^2
AZT	7.93	0.16	(0.13) – (0.37)	0.9700	0.293	3.41	2.44	0.7206
CEF	5.76	0.07	(0.25) – (0.57)	0.9676	0.431	2.32	0.92	0.9029

Adsorption Equilibrium Studies

It is well known that analyzing isotherm data before UV irradiation can be useful for finding a logical relationship between the adsorbed pollutant amount and its equilibrium concentration.[27, 28] Langmuir and Freundlich isotherms were utilized to examine the adsorption equilibrium conditions, and the results of both AZT and CEF pollutants are shown in Figure 9. Langmuir adsorption isotherm can be described by the following formula:[29, 30]
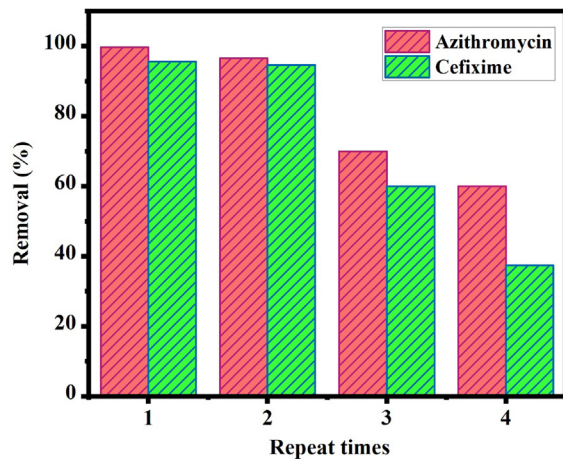
Figure 8: Recycling test on the PAC/Fe/Si/Zn nanocomposite for the UV-assisted removal of AZT and CEF.

$$\frac{C_e}{q_e} = \frac{1}{q_{max} K_L} + \frac{C_e}{q_{max}} \quad (6)$$

$$R_L = \frac{1}{1 + K_L C_0} \quad (7)$$

where C_0 and C_e (mgL^{-1}) stand for the initial and equilibrium concentration, respectively. q_e (mgg^{-1}) stands for the adsorption capacity, and q_{max} (Lmg^{-1}) stands for the maximum adsorption capacity. q_{max} describing the affinity of the binding sites is calculated from the intercept of the linear plot of C_e/q_e vs. C_e. K_L (mgg^{-1}) that is well-known as Langmuir constant, and can be also estimated from the slop of C_e/q_e vs. C_e. The Langmuir model would be favorable if the numerical value of R_L is placed between zero and one. However, a R_L value bigger than one shows that the Langmuir isotherm is unfavorable for the system under the study. Freundlich adsorption isotherm can be explained by the following formula:[31, 32]

$$\log q_e = \log K_F + \frac{1}{n_F} \log C_e \quad (8)$$

where K_F (mgg^{-1} or $(Lmg^{-1})^{1/n_F}$) describes the adsorption capacity and is calculated using the intercept of the plot of $\log q_e$ vs. $\log C_e$. Parameter 1/
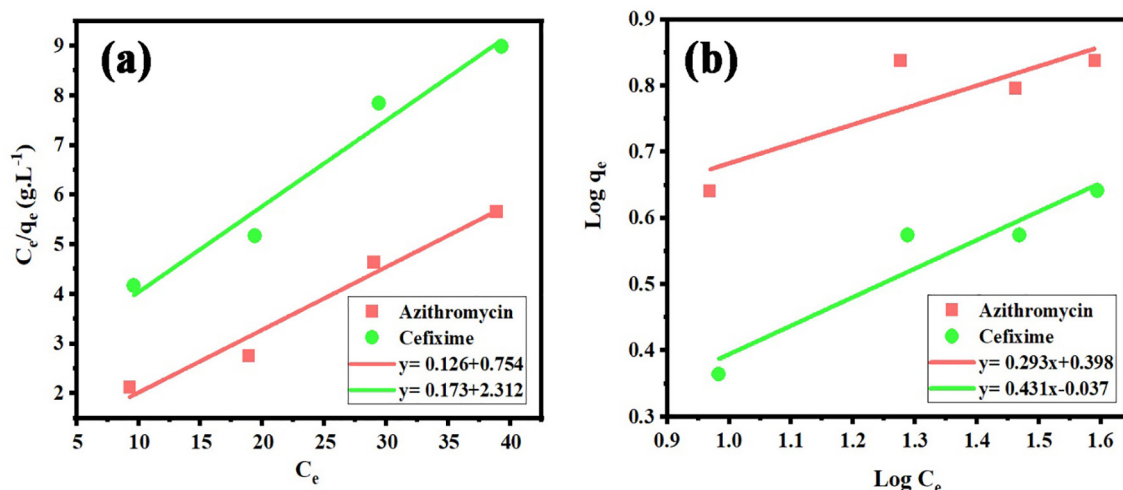
Figure 9: (a) Langmuir and (b) Freundlich plots for AZT/CEF adsorption using the PAC/Fe/Si/Zn nanocomposite

n_F stands for the adsorption intensity and is estimated from the slop of the line of log q_e vs. log C_e. The Freundlich adsorption isotherm would be favorable if n_F is placed between one and ten.[33]

Figure 9 plots adsorption equilibrium data obtained for the PAC/Fe/Si/Zn nanocomposite under optimized conditions estimated in UV-assisted removal processes. The adsorption equilibrium experiments were performed in solutions with initial AZT/CEF concentrations of 10, 20, 30 and 40 ppm. As shown in Figure 9, the experimental data have been presented by symbols, while the theoretical fits were given using solid lines. Table 3 summarizes the numerical data estimated using theoretical fits. As given in the Table, the R_L values for both AZT and CEF were estimated to be between zero and one, revealing a favorable Langmuir adsorption model on active sites of the PAC/Fe/Si/Zn nanocomposite with similar affinity. The Freundlich coefficients n_f were found to be between one and 10, indicating that Freundlich model was also favorable for the adsorption of both AZT and CEF on PAC/Fe/Si/Zn surfaces. It is shown in Table 3 that CEF adsorption on the surface of the PAC/Fe/Si/Zn nanocomposite was well fitted by both Langmuir and Freundlich models with high correlation coefficients. However, Langmuir isotherm with higher correlation coefficient was a more suitable adsorption model for AZT compared to Freundlich isotherm model.

Discussion

X-Ray diffraction test was used to characterize the synthesized sample. The results obtained from X-Ray diffraction test confirmed the presence of C, Si and Zn elements in PAC/Fe/Si/Zn sample. In order to study the morphology of the synthesized nanostructures, we used a filed-based scanning electron microscopy test (FESEM). The results showed a mixed morphology including fiber-like, sphere-like, and irregular shapes with average diameter of about 60 nm for fiber-like particles and few tens nm for sphere-like structures. The result of elemental mapping analysis showed the distribution of nanocomposite elements in the PAC/Fe/Ag/Zn nanostructures. The elements Si, activated carbon, zinc and iron are evenly distributed on the nanostructured surface and the elements are well dispersed.

The results showed that the efficiency of AZT and CEF removal increases by increasing amount of the absorbent. Increasing the amount of absorbent will increase the efficiency of AZT and CEF removal due to the specific and inner pores of absorbent.

pH is one of the most important parameters affecting the efficiency of pollutant removal in wastewater. The pH affects the adsorption capacity, degradation of target compound, distribution of electrical charge on the photocatalyst, and oxidation of the capacity band. A previous study has also showed that pH plays an important role in the removal of antibiotics. Results of Mohammed et al. about Tetracycline removal by using Pistachio shell coated with ZnO nanoparticles from wastewater revealed that the Tetracycline removal efficiency increased as the pH solution increased from 3 to 5. Greater removal efficiency (78.21%) was obtained at pH 5, while after pH 9, the efficiency decreased from 78.21 to 55.79%.[34]

In the present study, the amount of adsorption of AZT and CEF was increased by increasing the contact time. This is due to the increase in the probability of the collision of AZT and CEF molecules with absorptive surface. Gashtasbi et al. reported that when adsorbent dosage increased from 0.1 to 2 g/L, antibiotic removal efficiency showed an enhancing trend from 22.50 to 96.43%.[32]

By increasing the initial concentration of AZT and CEF, the removal efficiency is reduced. It means that with increasing the initial concentration of the contaminant, the removal efficiency is reduced, which is normal because with increasing the initial antibiotic concentration, the number of adsorption

sites remains constant compared to the increase in number of molecules of the adsorbed substance, and the adsorbent surface is saturated at high antibiotic concentrations; similar results have been observed in previous studies. Gashtasbi et al. reported that photocatalytic degradation of CEX witnessed a significant decline with increasing initial CEX concentration from 5 to 50 mg/L. In fact, at specific catalyst dosage, an increase in the initial contaminant concentrations leads to a decrease in its photocatalytic removal.[28]

The compatibility of the experimental data with isothermal models of Langmuir and Frendelich was investigated using correlation coefficient. Through comparing the values of correlation coefficient in the two models of isothermal Langmuir (R^2=0.97), *Freundlich Isotherm* (R^2=0.7206) for Azithromycin and isothermal Langmuir (R^2=0.9676), *Freundlich* (R^2=0.9029) for Cefixime, it is clear that isothermal Langmuir is more consistent with the data obtained in the present study for two antibiotics; also, the absorption of AZT and CEF on nano adsorbent PAC/Fe/Si/Zn is a single layer and distributed homogenous active sites on the absorbent surface. Huízar-Félix et al. about Removal of Tetracycline Pollutants by Adsorption for α-Fe2O3 Nanoparticles reported that adsorption fitted very well with the *Freundlich Isotherm* model, whereas the adsorption isotherm for α-Fe2O3/RGO fits better with the Langmuir model.[35]

Conclusion

The PAC/Fe/Si/Zn nanocomposite was successfully synthesized via loading iron (Fe), silicon (Si) and zinc (Zn) on powder activated carbon (PAC). The structural characteristics were analyzed using X-ray diffraction (XRD), field emission scanning electron microscopy (FESEM), and energy dispersive X-ray spectroscopy (EDS). The as-synthesized product was applied for the removal of azithromycin and cefixime from aqueous solutions by a UV system. The conditions of the UV-assisted reactions were optimized by changing pH, irradiation time, initial azithromycin/cefixime concentration, and nanocomposite dose. The results revealed higher removal efficiency of about 99.7% for azithromycin compared to the removal percentage for cefixime that was found to be about 95.6%.

The findings of kinetic studies using Langmuir-Hinshelwood model showed that UV-assisted removal had the best fit with the first-order kinetics for both azithromycin and cefixime. Adsorption equilibrium data were modeled using Langmuir and Freundlich isotherms. The isotherm models including Langmuir and Freundlich were valued and the equilibrium data were in agreement with both Langmuir and Freundlich models for the azithromycin adsorption, and by Langmuir isotherm for the cefixime removal. The

findings showed that PAC/Fe/Si/Zn Nano composite were well able to degrade non-biodegradable antibiotics in aqueous solutions, which is very valuable from an environmental aspects.

Conflict of Interest: No declared.

Reference

1   Peña-Guzmán C, Ulloa-Sánchez S, Mora K, Helena-Bustos R, Lopez-Barrera E, Alvarez J, Rodriguez-Pinzón M. Emerging pollutants in the urban water cycle in Latin America: A review of the current literature. Journal of environmental management. 2019; 237(1):408-23.

2   Jiang JQ, Zhou Z, Sharma VK. Occurrence, transportation, monitoring and treatment of emerging micro-pollutants in waste water—a review from global views. Microchemical Journal. 2013; 110(1):292-300.

3   Halling-Sørensen BN, Nielsen SN, Lanzky PF, Ingerslev F, Lützhøft HH, Jørgensen SE. Occurrence, fate and effects of pharmaceutical substances in the environment-A review. Chemosphere. 1998; 36(2): 357-93.

4   Kanda R, Griffin P, James HA, Fothergill J. Pharmaceutical and personal care products in sewage treatment works. Journal of Environmental Monitoring. 2003; 5(5):823-30.

5   Cano PA, Jaramillo-Baquero M, Zúñiga-Benítez H, Londoño YA, Peñuela GA. Use of simulated sunlight radiation and hydrogen peroxide in azithromycin removal from aqueous solutions: optimization & mineralization analysis. Emerging Contaminants. 2020; 6: 53-61.

6   Shokri R, Jalilzadeh Yengejeh R, Babaei AA, Derikvand E, Almasi A. Advanced Oxidation Process Efficiently Removes Ampicillin from Aqueous Solutions. Iranian Journal of Toxicology. 2020; 14(2): 123-4.

7   Muñoz-Calderón A, Zúñiga-Benítez H, Valencia SH, Rubio-Clemente A, Upegui SA, Peñuela GA. Use of low frequency ultrasound for water treatment: Data on azithromycin removal. Data in Brief. 2020; 31:105947.

8   Naraginti S, Yu YY, Fang Z, Yong YC. Visible light degradation of macrolide antibiotic azithromycin by novel ZrO2/Ag@ TiO2 nanorod composite: Transformation pathways and toxicity evaluation. Process Safety and Environmental Protection. 2019;125:39-49.

9   Sayadi MH, Sobhani S, Shekari H. Photocatalytic degradation of azithromycin using GO@ Fe3O4/ZnO/SnO2 nanocomposites. Journal of Cleaner Production.

2019; 232:127-36.

10 Shokri R, Jalilzadeh Yengejeh R, Babaei AA, Derikvand E, Almasi A. Removal of azithromycin from wastewater using advanced oxidation processes (UV/H2O2) and moving-bed biofilm reactor (MBBR) by the response surface methodology (RSM). Journal of Advances in Environmental Health Research. 2019;7(4):249-59.

11 Salimi M, Esrafili A, Jafari AJ, Gholami M, Sobhi HR, Nourbakhsh M, Akbari-Adergani B. Photocatalytic degradation of cefixime with MIL-125 (Ti)-mixed linker decorated by g-C3N4 under solar driven light irradiation. Colloids and Surfaces A: Physicochemical and Engineering Aspects. 2019; 582: 123874.

12 Salimi M, Esrafili A, Jafari AJ, Gholami M, Sobhi HR. Application of MIL-53 (Fe)/urchin-like g-C3N4 nanocomposite for efficient degradation of cefixime. Inorganic Chemistry Communications. 2020; 111: 107565.

13 Pham TD, Bui TT, Truong TT, Hoang TH, Le TS, Duong VD, Yamaguchi A, Kobayashi M, Adachi Y. Adsorption characteristics of beta-lactam cefixime onto nanosilica fabricated from rice HUSK with surface modification by polyelectrolyte. Journal of Molecular Liquids. 2020; 298: 111981.

14 Kim I, Yamashita N, Tanaka H. Performance of UV and UV/H2O2 processes for the removal of pharmaceuticals detected in secondary effluent of a sewage treatment plant in Japan. Journal of Hazardous Materials. 2009; 166(2-3): 1134-40.

15 Vogna D, Marotta R, Napolitano A, Andreozzi R, d'Ischia M. Advanced oxidation of the pharmaceutical drug diclofenac with UV/H2O2 and ozone. Water research. 2004; 38(2): 414-22.

16 Shokri R, Jalilzadeh Yengejeh R, Babaei AA, Derikvand E, Almasi A. Advanced Oxidation Process Efficiently Removes Ampicillin from Aqueous Solutions. Iranian Journal of Toxicology. 2020;14(2):123-4.

17 Fu Y, Gao X, Geng J, Li S, Wu G, Ren H. Degradation of three nonsteroidal anti-inflammatory drugs by UV/persulfate: degradation mechanisms, efficiency in effluents disposal. Chemical Engineering Journal. 2019; 356: 1032-41.

18 Li L, Gao NY, Deng Y, Yao JJ, Zhang KJ, Li HJ, Ou HS, Guo JW. Experimental and model comparisons of H 2 O 2 assisted UV photodegradation of Microcystin-LR in simulated drinking water. Journal of Zhejiang University-SCIENCE A. 2009; 10(11):1660-9.

19 Asgari G, Seidmohammadi A, Rahmani AR, Samarghandi MR, Faraji H. Application of the UV/sulfoxylate/phenol process in the simultaneous removal of nitrate and pentachlorophenol from the aqueous solution. Journal of Molecular Liquids. 2020; 314:113581.

20 Janssens R, Cristovao MB, Bronze MR, Crespo JG, Pereira VJ, Luis P. Coupling of nanofiltration and UV, UV/TiO2 and UV/H2O2 processes for the removal of anti-cancer drugs from real secondary wastewater effluent. Journal of Environmental Chemical Engineering. 2019;7(5):103351.

21 Mansour F, Al-Hindi M, Yahfoufi R, Ayoub GM, Ahmad MN. The use of activated carbon for the removal of pharmaceuticals from aqueous solutions: a review. Reviews in Environmental Science and Bio/Technology. 2018;17(1):109-45.

22 Kakavandi B, Kalantary RR, Farzadkia M, Mahvi AH, Esrafili A, Azari A, Yari AR, Javid AB. Enhanced chromium (VI) removal using activated carbon modified by zero valent iron and silver bimetallic nanoparticles. Journal of environmental health science and engineering. 2014;12(1):115.

23 Chawla S, Uppal H, Yadav M, Bahadur N, Singh N. Zinc peroxide nanomaterial as an adsorbent for removal of Congo red dye from waste water. Ecotoxicology and Environmental Safety. 2017; 135: 68-74.

24 Yoon KH, Noh JS, Kwon CH, Muhammed M. Photocatalytic behavior of TiO2 thin films prepared by sol–gel process. Materials Chemistry and Physics. 2006; 95(1):79-83.

25 Shang H, Lu Y, Zhao F, Chao C, Zhang B, Zhang H. Preparing high surface area porous carbon from biomass by carbonization in a molten salt medium. RSC advances. 2015;5(92):75728-34.

26 Sivakumar P, Kumar GG, Renganathan S. Synthesis and characterization of ZnS-Ag nanoballs and its application in photocatalytic dye degradation under visible light. Journal of Nanostructure in Chemistry. 2014; 4(3):107.

27 Zhang L, Li H, Liu Y, Tian Z, Yang B, Sun Z, Yan S. Adsorption-photocatalytic degradation of methyl orange over a facile one-step hydrothermally synthesized TiO 2/ZnO–NH 2–RGO nanocomposite. RSC Advances. 2014;4(89):48703-11.

28 Gashtasbi F, Yengejeh RJ, Babaei AA. Photocatalysis assisted by activated-carbon-impregnated magnetite composite for removal of cephalexin from aqueous solution. Korean Journal of Chemical Engineering. 2018;35(8):1726-34.

29 El-Moselhy MM, Kamal SM. Selective removal and preconcentration of methylene blue from polluted water using cation exchange polymeric material. Groundwater for Sustainable Development. 2018;6:6-13.

30 Nekouei F, Nekouei S. Comparative evaluation of BiOCl–NPls–AC composite performance for methylene blue dye removal from solution in the presence/absence of UV irradiation: Kinetic and isotherm studies. Journal of Alloys and Compounds. 2017;701:950-66.

31 Ali A, Mannan A, Hussain I, Hussain I, Zia M. Effective removal of metal ions from aquous solution by silver and zinc nanoparticles functionalized cellulose: isotherm, kinetics and statistical supposition of process. Environmental Nanotechnology, Monitoring & Management. 2018;9:1-11.

32 Gashtasbi F, Jalilzadeh Yengegeh R, Babaei AA. Adsorption of vancomycin antibiotic from aqueous solution using an activated carbon impregnated

magnetite composite. Des Water Treat. 2017;88:286-97.

33 Gunasundari E. Adsorption isotherm, kinetics and thermodynamic analysis of Cu (II) ions onto the dried algal biomass (Spirulina platensis). Journal of Industrial and Engineering Chemistry. 2017;56:129-44.

34 Mohammed AA, Kareem SL. Adsorption of tetracycline fom wastewater by using Pistachio shell coated with ZnO nanoparticles: Equilibrium, kinetic and isotherm studies. Alexandria Engineering Journal. 2019;58(3):917-28.

35 Huízar-Félix AM, Aguilar-Flores C, Martínez-de-la Cruz A, Barandiarán JM, Sepúlveda-Guzmán S, Cruz-Silva R. Removal of tetracycline pollutants by adsorption and magnetic separation using reduced graphene oxide decorated with α-Fe2O3 nanoparticles. Nanomaterials. 2019;9(3):313.